SCIEPublish

Article

Efficient Removal of Glyphosate from Aqueous Solution by Cerium Dioxide Loaded Biochar

Bo Zuo, Ruipu Wang, Jia Wang *, Junxia Yu *, Xiaodi Li, Li Guo, Yuchi Chen, Qingbiao Zhao, Chunqiao Xiao and Ruan Chi

Key Laboratory of Novel Biomass-Based Environmental and Energy Materials in Petroleum and Chemical Industry, Hubei Novel Reactor & Green Chemical Technology Key Laboratory, Key Laboratory for Green Chemical Process of Ministry of Education, School of Chemistry and Environmental Engineering, Wuhan Institute of Technology, No. 693 Xiongchu Avenue, Hongshan District, Wuhan 430074, China; 1097454802@qq.com (B.Z.); 1664958539@qq.com (R.W.); 1814759787@qq.com (X.L.); 718432836@qq.com (L.G.); 396075932@qq.com (Y.C.); 23031701@wit.edu.cn (Q.Z.); chunqiao@wit.edu.cn (C.X.); rac@wit.edu.cn (R.C.)

* Corresponding author. E-mail: jiawang@wit.edu.cn (J.W.); yujunxia_1979@163.com (J.Y.); Tel.: +86-02787194980 (J.W.); Fax: +86-02787194980 (J.W.)

Received: 13 November 2024; Accepted: 12 February 2025; Available online: 21 February 2025

ABSTRACT: Glyphosate, which is one of the most widely used organophosphorus herbicides, poses a threat to the surrounding water environment. Traditional adsorbents were depicted to have poor capacities to eliminate it. CeO_2 embraces the potential to adsorb glyphosate efficiently. However, suitable carbonaceous composites were necessary to be employed as its support. In this paper, water hyacinth was used as the precursor to prepare CeO_2-loaded biochar (CeO_2/WHBC), which was employed to remove glyphosate from the aqueous solution via adsorption. The results showed that CeO_2/WHBC-3 illustrated the best adsorption performance for glyphosate with the capacity of 126.3 mg·g, which was prepared with per mmol CeO_2 loaded of 0.2 g WHCB. Static adsorption experiments demonstrated that glyphosate adsorption at different solution pH values followed the Langmuir isotherm model and quasi-second order kinetic model, indicating that the adsorption was monolayer adsorption and that the adsorbent's surface active sites primarily controlled the rate. Coexisting ion interference experiments showed that common cations (K^+, Na^+, Ca^{2+}, Mg^{2+}) and anions (Cl^-, NO_3^-, SO_4^{2-}) both promoted glyphosate adsorption on the CeO_2/WHBC-3 surface. Moreover, the prepared sorbent maintained a high adsorption capacity after five adsorption-desorption cycles. Dynamic adsorption experiments showed that the CeO_2/WHBC-3 packed column could efficiently remove glyphosate from aqueous solutions, even at high concentrations and fast flow rates. Zeta potentials and XPS analysis revealed that the adsorption mechanism of CeO_2/WHBC-3 for glyphosate is mainly through electrostatic adsorption and metal complexation.

Keywords: Water hyacinth; Biochar; Glyphosate; Adsorption; CeO_2

© 2025 The authors. This is an open access article under the Creative Commons Attribution 4.0 International License (https://creativecommons.org/licenses/by/4.0/).

1. Introduction

Glyphosate, chemically known as N-(methyl phosphate) glycine, is a highly effective, broad-spectrum, and most widely used organophosphorus pesticide, mainly used for weeding non-cultivated land, including orchards, roads and forestry, and planting rice fields with little or no tillage. Due to its high efficiency, glyphosate become one of the most widely used organic phosphorus pesticides worldwide [1–3]. However, most glyphosate would be migrated into the water bodies via the rainfall. Its excessive use can lead to high concentrations in the aqueous solutions, which may negatively impact water quality and produce toxic effects on aquatic organisms. Therefore, research on glyphosate removal has gained increasing attention [4–8].

Currently, technologies such as advanced oxidation, chemical oxidation, chemical precipitation, biodegradation, membrane filtration, and adsorption are used to treat glyphosate-contaminated wastewater [9–11]. Among these technologies, adsorption offers advantages of high efficiency, ease of operation, and low cost [12–15]. Commonly used adsorbents include mesoporous materials such as metal compounds, activated carbon, industrial resins, and zeolites. As an emerging functional material, biochar can remove pollutants through physical and chemical adsorption [16–19]. Among carbonization technologies used to prepare biochar, slow pyrolysis was identified as the most efficient for

https://doi.org/10.70322/gct.2025.10002

achieving a satisfying yield and porous structure [20–22]. Additionally, using low-cost, naturally biodegradable waste biomass as a feedstock can potentially reduce operation costs [23,24]. Water hyacinth, a tropical plant widely distributed in the southern watersheds of China, is characterized by its rapid growth, prolific reproduction, and robust adaptability to different environments. However, water hyacinths can block sunlight, reduce dissolved oxygen levels in water and outcompete other aquatic plants. Composed of three carbon-based polymers-cellulose, hemicellulose, and lignin, water hyacinth is considered as a promising precursor of biochar [25,26]. Compared to other biomass sources, water hyacinth biochar has a larger pore size and specific surface area, making it suitable for wastewater treatment and mitigating ecological and environmental issues caused by its uncontrolled growth. Transformation of water hyacinth into biochar realized a "win-win" strategy to not only remediate environmental pollution but also recycle the ecological-harmful solid waste [27]. However, its limited adsorption capacity and non-selectivity hinder its widespread application in practical wastewater treatment [28,29]. Appropriate biochar modification is essential to improve its adsorption performance and selectivity [30–33].

Nanoparticle loading is an effective method of enhancing the selectivity and capacity of adsorbents. Commonly used nanoparticles include metal nanoparticles, oxide nanoparticles, carbon-based nanoparticles, and polymer nanoparticles. Considering their strong affinity for phosphate, rare earth elements (REEs) are prospective and highly selective adsorbents for phosphate removal [34,35]. Among these, cerium dioxide (CeO_2) is an inexpensive and sustainable rare earth oxide with stable and non-toxic chemical properties [36–38]. Cerium dioxide and its related adsorbents are gaining significant interest in their use in water treatment. The substantial surface charge, a variety of functional groups, and strong attraction to surface hydroxyls enable the rapid formation of cerium ion complexes with pollutants, including phosphates and arsenic, making cerium dioxide an excellent material for ecological remediation [39–42]. It has become a potential candidate for water purification. However, cerium (hydro)oxide exhibits low capacity and slow rate in phosphate adsorption, which restrain its practical applications. To improve the adsorption performance towards phosphate as well as reduce the usage of cerium, host materials, including biochar, porous silica micro-sphere and molecular sieve, were used to support and disperse cerium (hydro)oxide [43,44]. There are few reports on the preparation of ceria-loaded activated carbon and its application in the adsorption of glyphosate [45–49].

Herein, we present a recyclable CeO_2-based adsorbent capable of capturing and subsequently releasing glyphosate, facilitating its recovery and enabling the reuse of the adsorbent. In designing these adsorbents, we have exploited the exceptional binding capacity of cerium oxide nanostructures to load glyphosate onto biochar. Specifically, in this study, cerium dioxide-loaded water hyacinth biochar (CeO_2/WHBC) was synthesized using an *in situ* precipitation technique. The optimal preparation conditions were investigated, and the as-prepared sorbent was characterized by scanning electron microscope (SEM), X-ray diffraction (XRD), Fourier transform infrared (FTIR), X-ray photoelectron spectroscopy (XPS), and zeta potential analyses. The adsorption kinetics and isotherms of glyphosate on CeO_2/WHBC were studied, and the effects of solution pH, co-existing ions and regeneration processes on the adsorption performance of the sorbent were discussed. In addition, dynamic adsorption experiments and wastewater treatment tests were conducted to evaluate the potential applications of this adsorbent, which were further determined, and the adsorption mechanism was investigated.

2. Materials and Methods

2.1. Materials

Water hyacinth was purchased from Alibaba (Hangzhou, China), then washed, dried, ground, and sieved through 100–200 mesh before use. Chemical reagents, including sodium hydroxide, potassium hydroxide, concentrated hydrochloric acid, Cerium nitrate hexahydrate, glyphosate (99%), and absolute ethyl alcohol (all of analytical grade), were purchased from Sinopharm Chemical Reagent (Shanghai, China) and used without further purification.

2.2. Preparation and Characterization of CeO_2/WHBC-n

To remove soluble sugars and impurities, 14 g of water hyacinth was added to 500 mL of 1 $mol \cdot L^{-1}$ KOH. After stirring at room temperature for 20 min, the treated solid was separated and sequentially washed with distilled water and ethyl alcohol. To produce water hyacinth biochar (WHBC), the obtained water hyacinth was heated at a rate of 5 °C per minute from 30 °C to 500 °C and then calcined at this temperature for an hour in a tube furnace supplied with nitrogen. The solid product was further washed with 1 $mol \cdot L^{-1}$ HCl and hot distilled water, and it was then dried at 70 °C overnight prior to use.

The CeO_2/WHBC-n adsorbent was prepared by adding 0.10 g of WHBC to 50 mL of cerium nitrate solution at a concentration of 50.0 mmol·L^{-1}. After stirring the combination for half an hour at room temperature, a solution of 6 mol·L^{-1} NaOH was gradually added to adjust the solution pH to 12.0. The mixture was then stirred for a further hour, and the resulting sorbent was washed with distilled water and ethyl alcohol and then dried at 70 °C overnight before use. The cerium-containing particles were loaded onto the WHBC by adjusting the solution pH with NaOH. To investigate the effect of CeO_2 loading on the adsorption performance of glyphosate, CeO_2/WHBC adsorbents were prepared at $Ce(NO_3)_3$ concentrations of 2.0, 6.0, 10.0 and 20.0 mmol·L^{-1}. The physico-chemical properties of the prepared sorbents were analyzed using a scanning electron microscope (SEM, Hitachi S4800, Tokyo, Japan), an X-ray diffractometer (XRD, Rigaku D/max2500, Tokyo, Japan), X-ray photoelectron spectroscopy (XPS, Thermo Fisher Scientific Esca Lab 250Xi, Waltham, MA, USA), and a zeta potential analyzer (Zetasizer Nano Zs90, Malvern Instruments Ltd., Malvern, UK).

2.3. Batch Adsorption Experiments

Adsorption experiments were conducted at 25 °C with a shaker set to 250 rpm. To determine the adsorption isotherm, 0.010 g of adsorbent was added to 40.00 mL of glyphosate solution with a concentration range of 10–50 mg·L^{-1} at pH 3.4. For kinetic investigations, 0.050 g of adsorbent was mixed with 200.00 mL of 50 mg·L^{-1} glyphosate solution. In co-existence studies, 0.050 g of CeO_2/WHBC-3 was added to 200.00 mL of 50 mg·L^{-1} glyphosate solution containing co-existing cations. The initial concentrations of cations (K^+, Na^+, Ca^{2+}, Mg^{2+}) and anions (Cl^-, NO_3^-, SO_4^{2-}) ranging from 0 to 200 mg·L^{-1}. The influences of pH on adsorption performance were investigated in the range of 1.0 to 12.0. In the wastewater treatment experiment, CeO_2/WHBC-3 was added to a 40 mL solution containing 20 mg·L^{-1} glyphosate. Three adsorption-desorption cycles were performed to determine the reusability of the sorbents. For regeneration, 0.01 mg·L^{-1} NaOH was used, followed by washing with distilled water until neutral.

To determine the glyphosate concentration before and after adsorption, glyphosate was oxidized to phosphate using potassium persulfate as the oxidant and the resulting phosphate content was measured using ammonium molybdate spectrophotometry [50].

The quantity of glyphosate adsorbed was calculated using the following Equation (1): q_e (mg·g^{-1}) represents the amount of glyphosate adsorbed per unit mass of the sorbent, V (mL) is the volume of the glyphosate solution, C_0 (mg·L^{-1}) and C_e (mg·L^{-1}) is the concentration of glyphosate before and after adsorption, and m (g) is the weight of the adsorbent.

$$q_e = \frac{v(C_0 - C_e)}{m} \quad (1)$$

2.4. Dynamic Adsorption Experiments of Glyphosate on CeO_2/WHBC-3 Fixed Bed Column

Dynamic adsorption studies were conducted in a laboratory-scale fixed-bed column with an internal diameter of 1 cm and a height of 20 cm. Typically, 1.0 g of CeO_2/WHBC-3 was placed in the column, and glyphosate solution (0.50, 1.00, 1.2 mmol·L^{-1}) was passed through the column at varying flow rates (2.0, 3.0, 5.0 mL·min^{-1}). In the wastewater treatment experiment, simulated wastewater was prepared using glyphosate and running water, with a glyphosate concentration of 0.5 mmol·L^{-1} and a flow rate of 5 mL·min^{-1}. Samples were collected at various intervals, and glyphosate concentrations were evaluated using the same procedure as in the batch adsorption studies.

3. Results and Discussion

3.1. Preparation and Characterization of CeO_2/WHBC

Water hyacinth was firstly carbonized at 500 °C, and Figure 1 shows the adsorption capacity of glyphosate on CeO_2/WHBC at different loading levels. The adsorption capacities of CeO_2/WHBC prepared at $Ce(NO_3)_3$ concentrations of 2.0, 6.0, 10.0 and 20.0 mmol·L^{-1} were 60.7, 108.9, 126.3, and 109.4 mg·g^{-1}, respectively. The results indicated that the best adsorption performance was achieved with a $Ce(NO_3)_3$ solution of 10.0 mmol·L^{-1}. The corresponding adsorbents are CeO_2/WHBC-1, CeO_2/WHBC-2, CeO_2/WHBC-3 and CeO_2/WHBC-4, respectively. Therefore, CeO_2/WHBC-3 was selected as the adsorbent for the subsequent adsorption experiments.

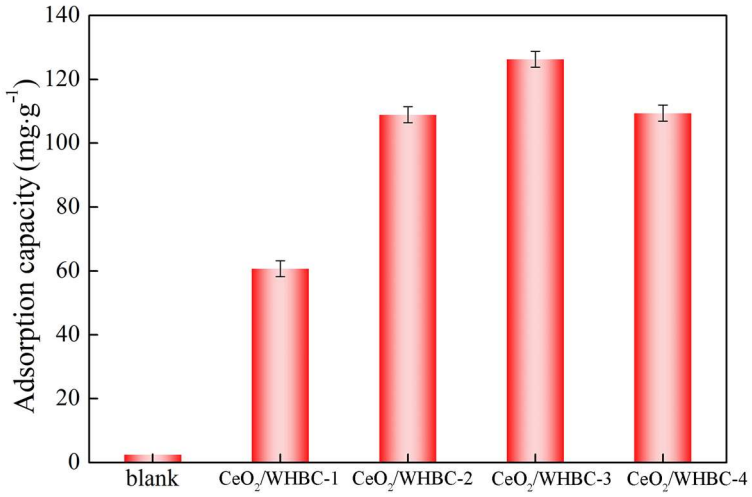

Figure 1. Adsorption capacity of CeO_2/WHBC with different CeO_2 loading amounts.

Since the adsorption capacity of glyphosate by CeO_2/WHBC varied significantly with different loadings, and this phenomenon might be related to the distribution of CeO_2 on the surface of the biochar, WHBC, CeO_2/WHBC-1, CeO_2/WHBC-3, and CeO_2/WHBC-4 were selected for SEM analysis, and the results are shown in Figure 2. From the figure, it can be seen that almost no CeO_2 nanoparticles were observed on the surface of the CeO_2/WHBC-1. However, when the loading amount was increased to a large number of CeO_2 nanoparticles were encapsulated on the biochar surface, and the original pore structure of the biochar was barely visible. Figure 2e shows the XRD patterns of biochar with different Ce loadings. The diffraction peaks of WHBC appear in the 20–30° and 40–50° intervals, which can be categorized as typical of an amorphous graphitic phase carbon material. It can also be observed that the crystallinity of CeO_2 on the surface of biochar gradually increases with higher loading amounts. When this adsorbent was CeO_2/WHBC-1, new diffraction peaks at 28°, 47° and 56° appeared in the XRD patterns, corresponding to the (111), (220), and (311) crystal planes of CeO_2, respectively. However, these three peaks were broad, indicating that the crystallinity of CeO_2 obtained at a low loading amount was poor. When this adsorbent was CeO_2/WHBC-3 and CeO_2/WHBC-4 the characteristic peaks of CeO_2 became sharp, and three diffraction peaks at 33°, 69°, and 76° were observed, corresponding to the (200), (400), and (331) crystal planes of CeO_2, respectively. This indicates that the CeO_2 loaded on the surface of biochar exhibited a cubic fluorite structure. Figure 2f shows the FTIR spectra of CeO_2/WHBC-3 before and after glyphosate adsorption. The absorption peak at 1066 cm^{-1} can be attributed to the bending vibration peak of Ce-OH on the surface of CeO_2, while the two absorption peaks located at 421 cm^{-1} and 853 cm^{-1} correspond to the characteristic stretching vibrations of Ce–O. Figure 2g presents the zeta potentials of WHBC and CeO_2/WHBC-3 before and after adsorption. The zeta potential of the biochar changed significantly after loading, with the isoelectric point increasing from 2.11 to 5.51. This shift indicates that CeO_2 introduced more positive charge sites on the material's surface, facilitating the adsorption of glyphosate on CeO_2/WHBC-3 [40].

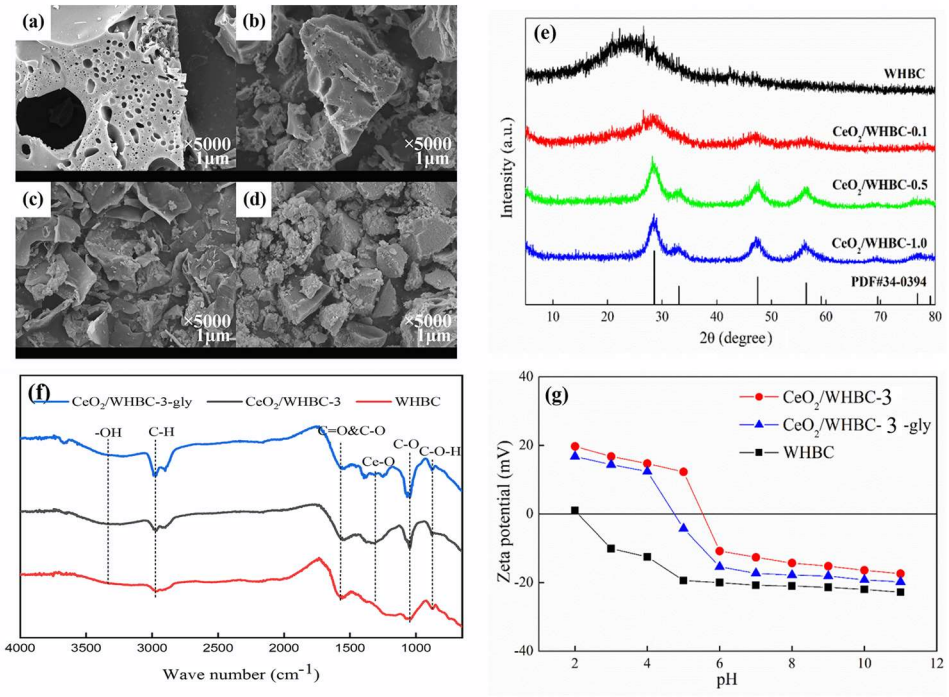

Figure 2. SEM of WHBC (**a**), CeO_2/WHBC-1 (**b**), CeO_2/WHBC-3 (**c**) and CeO_2/WHBC-4 (**d**), and (**e**) XRD of WHBC, CeO_2/WHBC-1, CeO_2/WHBC-3 and CeO_2/WHBC-4, (**f**) FTIR of CeO_2/WHBC-3 before and after glyphosate adsorption, (**g**) Zeta potential of WHBC, CeO_2/WHBC-3 before and after glyphosate.

3.2. Adsorption Isotherms and Kinetics of Glyphosate on CeO_2/WHBC-3

Since the pH of the system strongly influences the adsorption performance of glyphosate on CeO_2/WHBC-3, we investigated the isothermal adsorption of glyphosate by CeO_2/WHBC-3 at pH levels 1.0, 2.0, 4.0, 8.0 and 12.0. The results are shown in Figure 3. As shown in the figure, the adsorption of glyphosate by CeO_2/WHBC-3 increased gradually until reaching equilibrium with the rising initial concentration of glyphosate. The optimal pH for the adsorption performance of CeO_2/WHBC-3 to glyphosate was 2.0, followed by 4.0, 1.0, 8.0 and 12.0, aligning with the findings from experiments on the effect of acidity on the adsorption performance. The isothermal adsorption data at different pH levels were fitted to the Langmuir, Freundlich and Temkin isothermal adsorption models (Equations (2)–(4)), The q_e represents the equilibrium adsorption capacity of glyphosate ($mg \cdot g^{-1}$); q_m is the maximum adsorption capacity ($mg \cdot g^{-1}$); C_e is the equilibrium concentration of glyphosate ($mg \cdot L^{-1}$); K_L is the Langmuir adsorption constant ($L \cdot mg^{-1}$); K_F and $1/n$ are Freundlich adsorption constants ($mg \cdot mg^{-1/n} \cdot L^{1/n} \cdot g^{-1}$), which are related to the adsorption intensity between adsorbent and adsorbate; A_T ($L \cdot mg^{-1}$) is the maximum binding energy corresponding to the equilibrium binding constant; b_T is the Temkin isothermal constant ($mg^{-1} \cdot g^{-1}$); R and T represent the ideal gas constant (8.3145 $J \cdot mol^{-1} \cdot K^{-1}$) and temperature (K), respectively. The fitting results are presented in Table 1. The correlation coefficient (R^2) values fitted by the Langmuir model were much higher than those by the Freundlich and Temkin model. Based on the aforementioned results, it can be concluded that the Langmuir model more accurately describes the adsorption behaviour of glyphosate as compared to the Freundlich and Temkin models do, indicating that the adsorption of glyphosate on CeO_2/WHBC-3 follows a monomolecular layer chemisorption. The maximum adsorption capacities of glyphosate by CeO_2/WHBC-3 at pH levels of 1.0, 2.0, 4.0, 8.0, and 12.0 were 105.6, 122.6, 119.1, 30.2, and 3.9 $mg \cdot g^{-1}$, respectively, as calculated from the Langmuir model. A comparison with other carbon-based adsorbents reported in related literature (Table 2) reveals that CeO_2/WHBC-3 demonstrates superior adsorption performance for glyphosate in acidic conditions, suggesting its potential application in the treatment of acidic glyphosate wastewater. The pH of the static adsorption system influences not only the equilibrium form of glyphosate in the aqueous solution but also the surface charge of the adsorbent [32]. Figure 4 shows the adsorption capacity of CeO_2/WHBC-3 for glyphosate at various pH levels, indicating that glyphosate adsorption by CeO_2/WHBC-3 was more effective in the acidic conditions, whereas a significant decrease in adsorption capacity was observed under alkaline conditions. At pH levels of 2.0 and 4.0, as shown in Figure 2g, glyphosate is negatively charged, while CeO_2/WHBC-3 is positively charged, enabling the adsorption process to occur via electrostatic attraction. As the pH increased to 8.0 and 12.0, the zeta

potential diagram indicates that the pH exceeded the isoelectric point of the adsorbent, resulting in a negatively charged surface on CeO_2/WHBC-3. Consequently, the adsorption capacity of the adsorbent for glyphosate decreased significantly.

$$q_e = \frac{q_m K_L C_e}{1 + K_L C_e} \tag{2}$$

$$q_{e=} K_F C_e^{1/n} \tag{3}$$

$$q_e = \frac{RT}{b_T} \ln (A_T C_e) \tag{4}$$

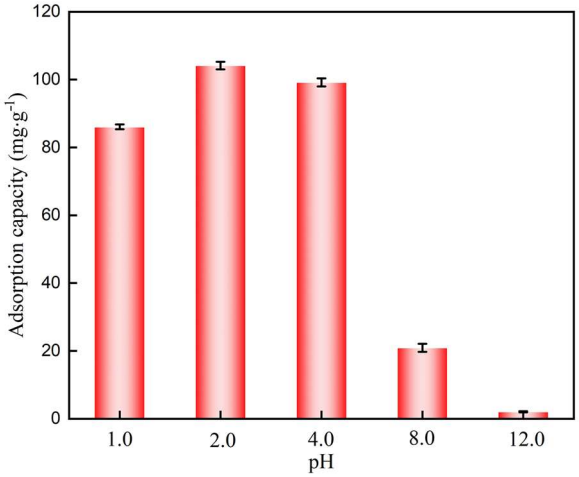

Figure 3. Effects of pH on adsorption performance of CeO_2/WHBC-3.

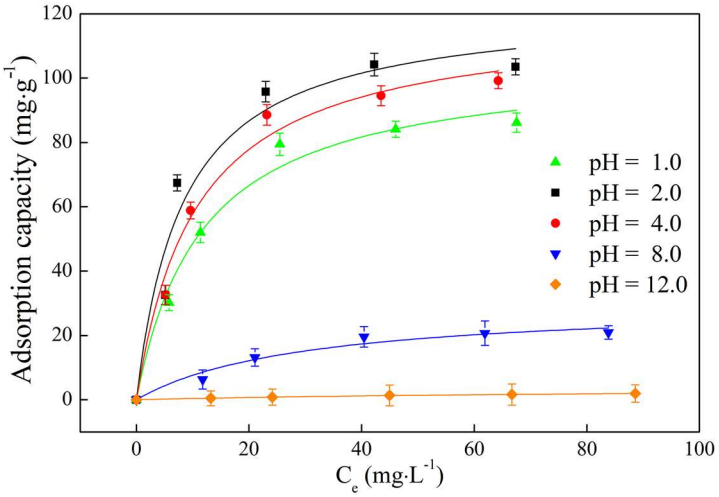

Figure 4. Adsorption isotherms of glyphosate on CeO_2/WHBC-3 at different Ph.

Table 1. Adsorption isotherm parameters fitted by Langmuir, Freundlich and Temkin models.

Model	Langmuir			Freundlich			Temkin		
pH	$1/K_L$	q_m	R^2	K_F	$1/n$	R^2	A_T	b_T	R^2
	mg·L^{-1}	mg·g^{-1}		(mg·g^{-1}) (L·mg^{-1})$^{1/n}$			L·mg^{-1}	J·mol^{-1}	
1.0	11.73	105.6	0.9818	22.1	0.342	0.8224	0.764	105.4	0.9103
2.0	8.28	122.6	0.9492	32.0	0.301	0.7214	1.23	96.6	0.8077
4.0	10.60	119.1	0.9831	25.7	0.341	0.8329	0.849	93.9	0.9189
8.0	29.75	30.2	0.9949	3.04	0.456	0.7968	0.236	324.4	0.9002
12.0	92.97	3.9	0.9598	0.09	0.683	0.9769	0.127	3194.4	0.9856

Table 2. Comparison of capacities among different carbon-based sorbents for glyphosate.

Adsorbent	Adsorption Conditions	q_m (mg·g^{-1})	Reference
$MnFe_2O_4$–G	pH = 4.0, 1.0 g·L^{-1}	39.0	[51]
Dendro biochar	pH = 4.0, 1.0 g·L^{-1}	44	[38]
MWCNT/MPNs-Fe	pH = 4.0, 1.5 g·L^{-1}	43.7	[40]
AC@AgNPs	pH = 3.8, 0.1 g·L^{-1}	149.3	[6]
Clay-biochar composite	pH = 8.0, 0.2 g·L^{-1}	37.1	[5]
BC-NZV	pH = 4.0, 0.6 g·L^{-1}	80	[29]
RHBC	pH = 4.0, 0.5 g·L^{-1}	30.5	[39]
$MnFe_2O_4$-CAC	pH = 3.4, 0.5 g·L^{-1}	162.7	[32]
$MnFe_2O_4$-PAC	pH = 4.0, 4 g·L^{-1}	119.6	[52]
MWCNT-COOH	pH = 4.0, 1.5 g·L^{-1}	21.2	[2]
CeO_2/WHBC	pH = 2.0, 0.25 g·L^{-1}	122.6	This study

The adsorption kinetics were also used to evaluate the adsorption performance of CeO_2/WHBC-3, as shown in Figure 5. It can be observed that the adsorption rate was faster within the first 5 min at different pH levels, with more than 90% of glyphosate adsorbed by CeO_2/WHBC-3. As the adsorption process continued from 5 to 30 min, the concentration of glyphosate gradually decreased as the active adsorption sites on the surface of the adsorbent became occupied, leading to a gradual reduction of the adsorption rate. The rate eventually stabilized and reached equilibrium within 60 min. To further investigate the adsorption behaviour of CeO_2/WHBC-3 on glyphosate, the pseudo-first-order model and the pseudo-second-order model were applied to fit the experimental data (Equations (5) and (6)), where q_e (mg·g^{-1}) and q_t (mg·g^{-1}) is the amount of glyphosate absorbed at equilibrium and time t, k_1 (min^{-1}) and k_2 (g·mg^{-1}·min^{-1}) is the rate constant of pseudo-first-order and pseudo-second-order model, respectively. The fitting results are presented in Table 3. Table 3 shows that the correlation coefficients (R^2) for glyphosate adsorption kinetics, fitted using the pseudo-second order model at pH levels 1.0, 2.0, 4.0, 8.0 and 12.0 were 0.9955, 0.9950, 0.9995, 0.9986 and 0.9937, respectively, which were much higher than those by the pseudo-first order model. This result indicates that the pseudo-second-order model describes the adsorption behavior of glyphosate more accurately than the pseudo-first-order model does, suggesting that the adsorption of glyphosate by CeO_2/WHBC-3 may be a chemisorption process controlled by the adsorption rate of the adsorption active sites [53]. The equilibrium adsorption capacities of glyphosate by CeO_2/WHBC-3 at pH 1.0, 2.0, 4.0, 8.0 and 12.0 were 83.7, 104.8, 98.8, 20.6 and 3.0, respectively, aligning more closely with the actual adsorption amounts than those predicted by the pseudo-first-order model.

$$q_t = q_e(1 - e^{-k_1 t}) \tag{5}$$

$$q_t = \frac{k_2 q e^2 t}{1 + k_2 q_e t} \tag{6}$$

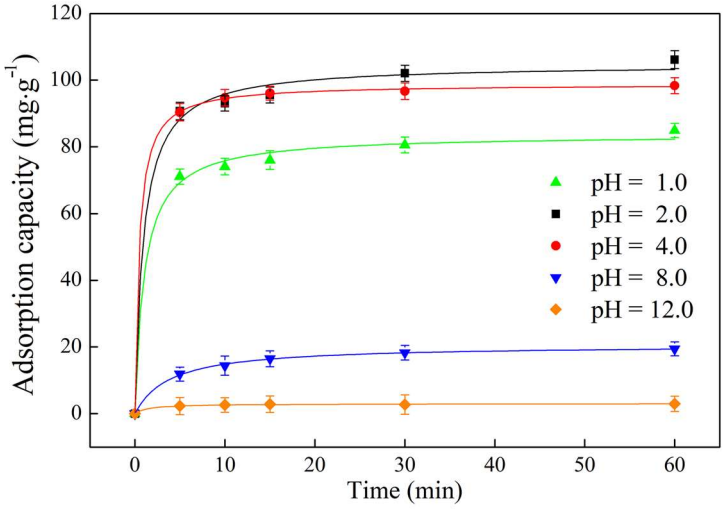

Figure 5. Adsorption kinetics of glyphosate on CeO_2/WHBC-3 at different pH.

Table 3. Adsorption kinetic parameters fitted by two kinetic models.

Model	Pseudo-First-Order Model			Pseudo-Second-Order Model		
pH	k_1 / min^{-1}	q_e / $mg \cdot g^{-1}$	R^2	k_2 / $g \cdot mg^{-1} \cdot min^{-1}$	q_e / $mg \cdot g^{-1}$	R^2
1.0	0.423	79.5	0.9849	1.04	83.7	0.9955
2.0	0.452	99.8	0.9850	0.94	104.8	0.9950
4.0	0.541	96.6	0.9991	0.45	98.8	0.9995
8.0	0.174	18.5	0.9834	3.88	20.6	0.9986
12.0	0.313	2.85	0.9926	1.50	3.01	0.9937

3.3. Effects of Co-Ions on Glyphosate Adsorption on CeO_2/WHBC-3

In the actual wastewater treatment process, a variety of co-existing ions (e.g., anions such as SO_4^{2-}, NO_3^- and Cl^- and cations such as Na^+, K^+, Ca^{2+} and Mg^{2+}) may compete with glyphosate for adsorption on the adsorbent surface, potentially affecting the amount of glyphosate adsorbed. This effect may vary depending on the concentration of the co-existing ions. Therefore, we investigated the effect of the CeO_2/WHBC-3 system in the presence of various concentrations of different interfering ions on the adsorption capacity for glyphosate, with the results shown in Figure 6. The figure reveals that the co-existing ions had little effect on the adsorption of glyphosate, indicating that the material has strong anti-interference ability.

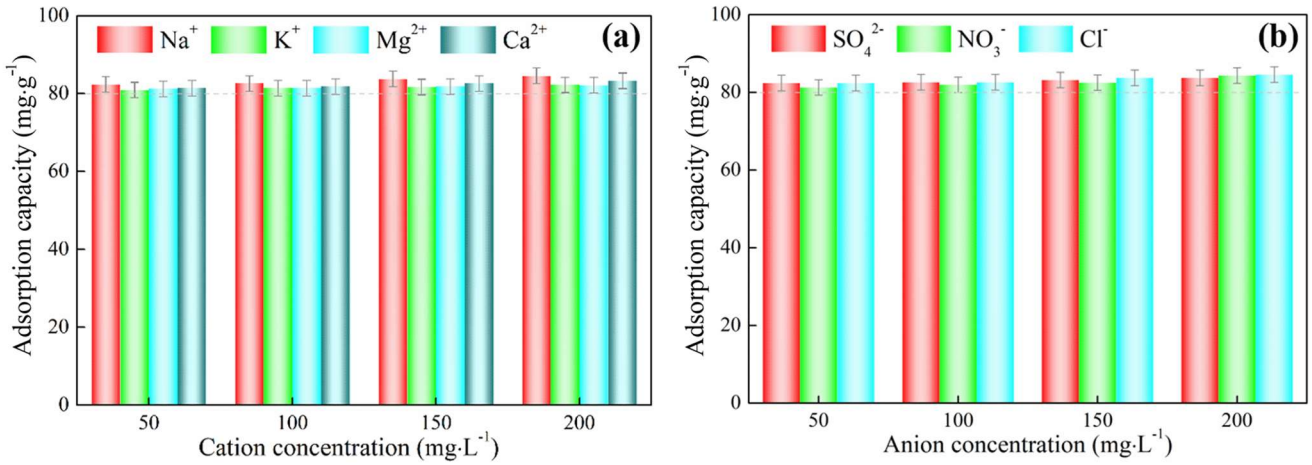

Figure 6. Effects of (**a**) cations and (**b**) anions on glyphosate adsorption on CeO_2/WHBC-3.

3.4. Cyclic Regeneration Performance of CeO_2/WHBC-3

To investigate the cyclic regeneration performance of the prepared adsorbent, we added 0.050 g of CeO_2/WHBC-3 to 200 mL of 50 $mg \cdot L^{-1}$ glyphosate solution, then regenerated the adsorbent using a 0.01 $mol \cdot L^{-1}$ NaOH solution before starting the next cycle. The results of the cyclic regeneration experiments, shown in Figure 7, indicate that CeO_2/WHBC-3 maintains strong adsorption performance for glyphosate even after five adsorption-desorption cycles, with a recovery rate over 90% using a 0.01 $mol \cdot L^{-1}$ NaOH solution. This suggests that the prepared CeO_2/WHBC-3 has significant potential for practical application.

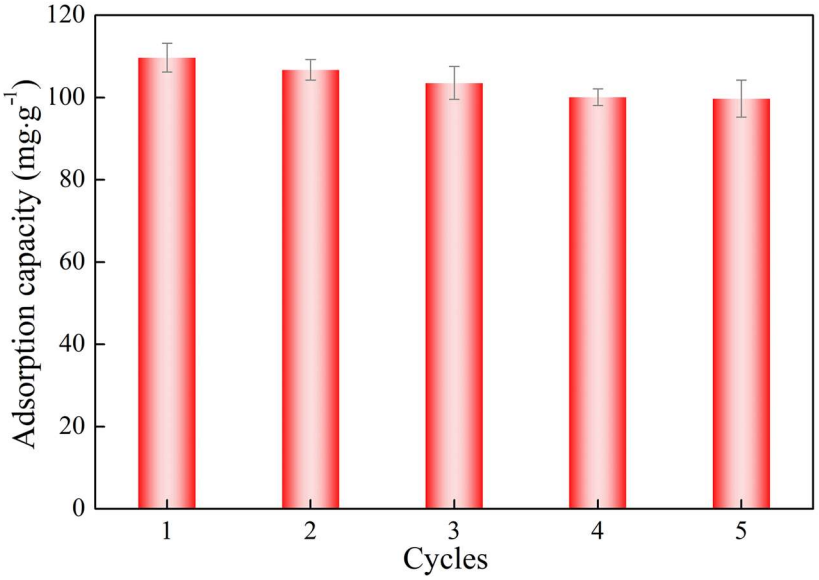

Figure 7. The reusability of CeO_2/WHBC-3.

3.5. Dynamic Adsorption of Glyphosate on CeO_2/WHBC-3

Dynamic adsorption is the predominant technique used in practical wastewater treatment processes, where flow rate and initial concentration are crucial factors influencing the effectiveness of glyphosate adsorption. The dynamic adsorption breakthrough curves of glyphosate on CeO_2/WHBC-3 at various flow rates and initial concentrations were examined, as shown in Figure 8a,c. During the initial phase of dynamic adsorption, a significant number of active sites on the adsorbent surface were occupied by glyphosate, resulting in C_t/C_0 values close to zero for the first 30 min.

As the active sites on the adsorbent surface became saturated with glyphosate, the packed column gradually approaching saturation, resulting in a rapid increase in C_t/C_0 to 1, indicating the attainment of adsorption equilibrium. As a result, the adsorption and breakthrough curves displayed an S-shaped profile across varying concentrations and flow rates. The breakthrough time ($C_t/C_0 < 0.05$) and the time to reach adsorption equilibrium decreased as the flow rate and initial concentration increased. For instance, increasing the flow rate from 2.0 mL·min^{-1} to 3.0 mL·min^{-1} and then to 5.0 mL·min^{-1} reduced the breakthrough time from 84.8 min to 58.2 min and further to 53.1 min, while the time to reach saturation reduced from 174.5 min to 129.1 min and then to 109.1 min. Similarly, when the initial concentration increased from 0.5 mmol·L^{-1} to 1.0 mmol·L^{-1} and then to 1.2 mmol·L^{-1}, the breakthrough time decreased from 53.1 min to 41.1 min and then to 31.2 min, while the saturation adsorption time shortened from 109.1 min to 70.8 min and finally to 63.3 min.

The adsorption capacity of glyphosate on CeO_2/WHBC-3 column at various flow rates and concentrations was calculated using Equation (7), with adsorption capacity over time curves shown in Figure 8b,d, respectively. As illustrated, the adsorption capacity of glyphosate on the CeO_2/WHBC-3 column initially increased linearly with time, then gradually levelled off as the column approached saturation and the adsorption equilibrium was achieved.

In a dynamic packed column, the adsorption capacity of glyphosate on CeO_2/WHBC-3 increased to 37.9, 51.0, and 59.6 mg·g^{-1} at flow rates of 2.0, 3.0, and 5.0 mL·min^{-1}, respectively. Similarly, at glyphosate concentrations of 0.5, 1.0, and 1.2 mmol·L^{-1}, the adsorption capacities were 59.6, 69.2, and 78.2 mg·g^{-1}, respectively. The findings suggest that adsorption efficiency improves with higher flow rates and concentrations, indicating that CeO_2/WHBC-3 is effective for treating glyphosate-laden wastewater at high initial concentrations and rapid flow rates.

In a more in-depth analysis of the adsorption process in the dynamic packed column, we applied the Bohart-Adams and Yoon-Nelson models to various breakthrough curves (Equations (8) and (9)), with the results detailed in Table 4. The Yoon-Nelson model parameters indicated that the constant adsorption rate constant KYN dropped from 0.14 to 0.09 min^{-1} with an increase in flow rate from 2.0 mL·min^{-1} to 5 mL·min^{-1}. Additionally, the times (τ\tauτ) required for half of the adsorbate to be adsorbed at flow rates of 2.0, 3.0, and 5.0 mL·min^{-1} were 119.7, 84.9, and 74.9 min, respectively. These findings suggest a direct relationship between the flow rate and the adsorption rate of glyphosate within the column.

$$q_t = \frac{v\int_0^t (C_0 - C_t)d_t}{m} \tag{7}$$

$$\frac{C_t}{C_0} = \frac{e^K AB^{C_0 t}}{e^K AB^{N_0 Z/V} - 1 + e^{K_{AB} C_0 t}} \tag{8}$$

$$\frac{C_t}{C_0} = \frac{1}{1 + e^{K_{YN}(t-\tau)}} \tag{9}$$

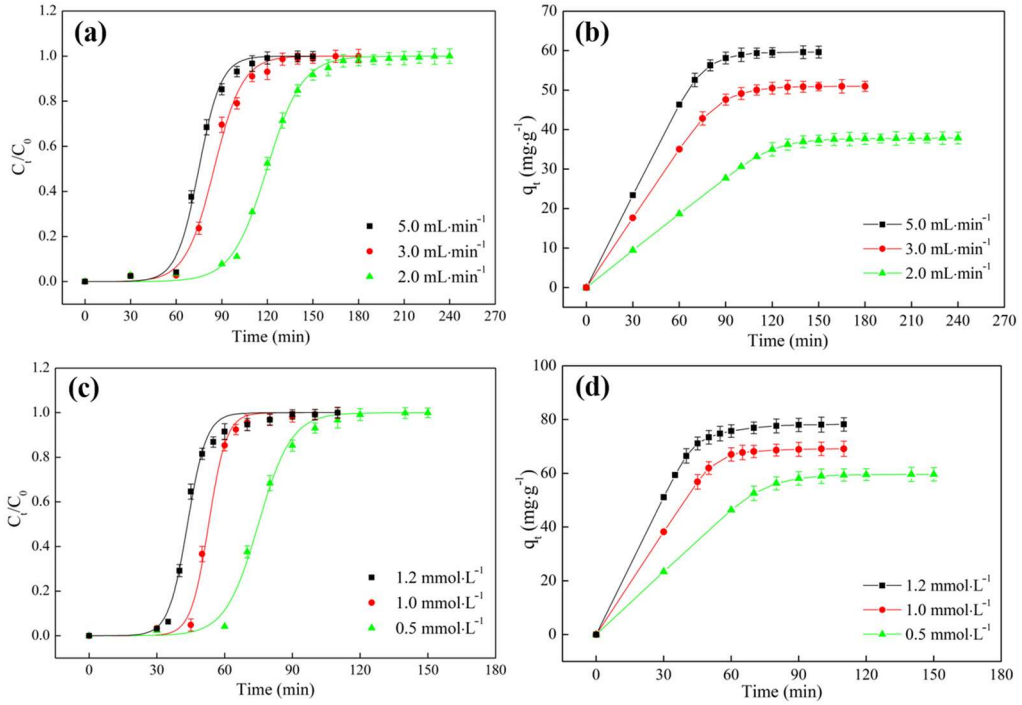

Figure 8. Effect of (**a**,**b**) flow rate and (**c**,**d**) initial concentration on the breakthrough curve and dynamic adsorption kinetics of glyphosate on the fixed bed column.

Table 4. Fitted parameters of the breakthrough curves at different flow rates and initial concentrations.

Model	**Bohart-Adams Model**			**Yoon–Nelson Model**			
Flow rate (mL·min^{-1})	K_{AB}	N_0	R^2	K_{YN}	τ	R^2	q_e
	L·mg^{-1}·min^{-1}	mg·L^{-1}		min^{-1}	min		(mg·g^{-1})
5.0	0.0018	352.6	0.9934	0.14	74.9	0.9934	59.6
3.0	0.0014	108.8	0.9941	0.11	84.9	0.9942	51.0
2.0	0.0011	396.9	0.9982	0.09	119.7	0.9982	37.9
Concentration (mmol·L^{-1})	K_{AB}	N_0	R^2	K_{YN}	τ	R^2	q_e
	L·mg^{-1}·min^{-1}	mg·L^{-1}		min^{-1}	min		(mg·g^{-1})
1.2	0.0011	150.7	0.9892	0.24	43.5	0.9892	78.2
1.0	0.0013	374.1	0.9937	0.25	52.9	0.9939	69.2
0.5	0.0018	352.6	0.9934	0.14	74.9	0.9934	59.6

3.6. Adsorption Mechanisms

The adsorption purification method for glyphosate treatment in solution is shown in Figure 9. Experiments on acidity and co-existing ions indicated that the adsorption of glyphosate by CeO_2/WHBC-3 primarily occurs through electrostatic attraction and inner-sphere complexation [15]. CeO_2/WHBC-3 was characterized before and after adsorption using zeta potential analysis, FTIR and XPS to support the conclusions. Isothermal and kinetic data at different pH levels indicate that CeO_2/WHBC-3 exhibits superior adsorption performance for glyphosate at pH ≤ 4.0. However, when the system's pH exceeds the isoelectric point of the adsorbent, the adsorption capacity for glyphosate significantly decreases, demonstrating a strong pH dependency in the adsorption process. Zeta potential analysis in

Figure 2g shows that the isoelectric point of the adsorbent decreased from 5.51 to 4.72 after adsorption, suggesting that the positively charged sites on the adsorbent surface are involved in the adsorption mechanism. This finding implies that the adsorption of glyphosate by CeO_2/WHBC-3 primarily occurs through electrostatic attraction. Additionally, FTIR and XPS characterization of CeO_2/WHBC-3 before and after adsorption further supports these findings. Figure 2f shows noticeable changes in the absorption peak of Ce-O at 421 cm^{-1} before and after adsorption, suggesting that Ce-OH and Ce-O groups on the adsorbent surface participate in the adsorption of glyphosate by hydrogen bonding [15]. Additionally, the enhanced absorption peaks at 1046 cm^{-1} and 878 cm^{-1} may correspond to the $H_2PO_3^-$ and P-OH structures present in glyphosate, suggesting the successful adsorption of glyphosate. The XPS spectrum of CeO_2/WHBC-3 before and after adsorption is shown in Figure 10. In the Ce 3d spectrum shown in Figure 10c, the binding energies at 882.7, 889.0, 898.6, 903.8, 907.58 and 917.0 eV are attributed to Ce^{4+}, while those at 901.2 and 885.7 eV correspond to Ce^{3+}. After adsorption, the Ce 3d peak at 898.6 eV shifted to 898.8 eV, indicating a higher binding energy, which suggests that Ce^{4+} on the adsorbent surface may form a Ce-O-P complex structure. The peak at the binding energy of 531.7 eV in the O 1s XPS spectrum in Figure 10b can be attributed to Ce-OH on the CeO_2 surface, while the peak at 529.8 eV corresponds to Ce-O within the lattice. After adsorption, the Ce-OH peak at 531.7 eV shifts to 531.8 eV, indicating a higher binding energy. Additionally, a new peak appears in the P 2p XPS spectrum in Figure 10d at 133.3 eV. These results suggest that the hydroxyl groups on the surface of CeO_2 are involved in the glyphosate adsorption process [21].

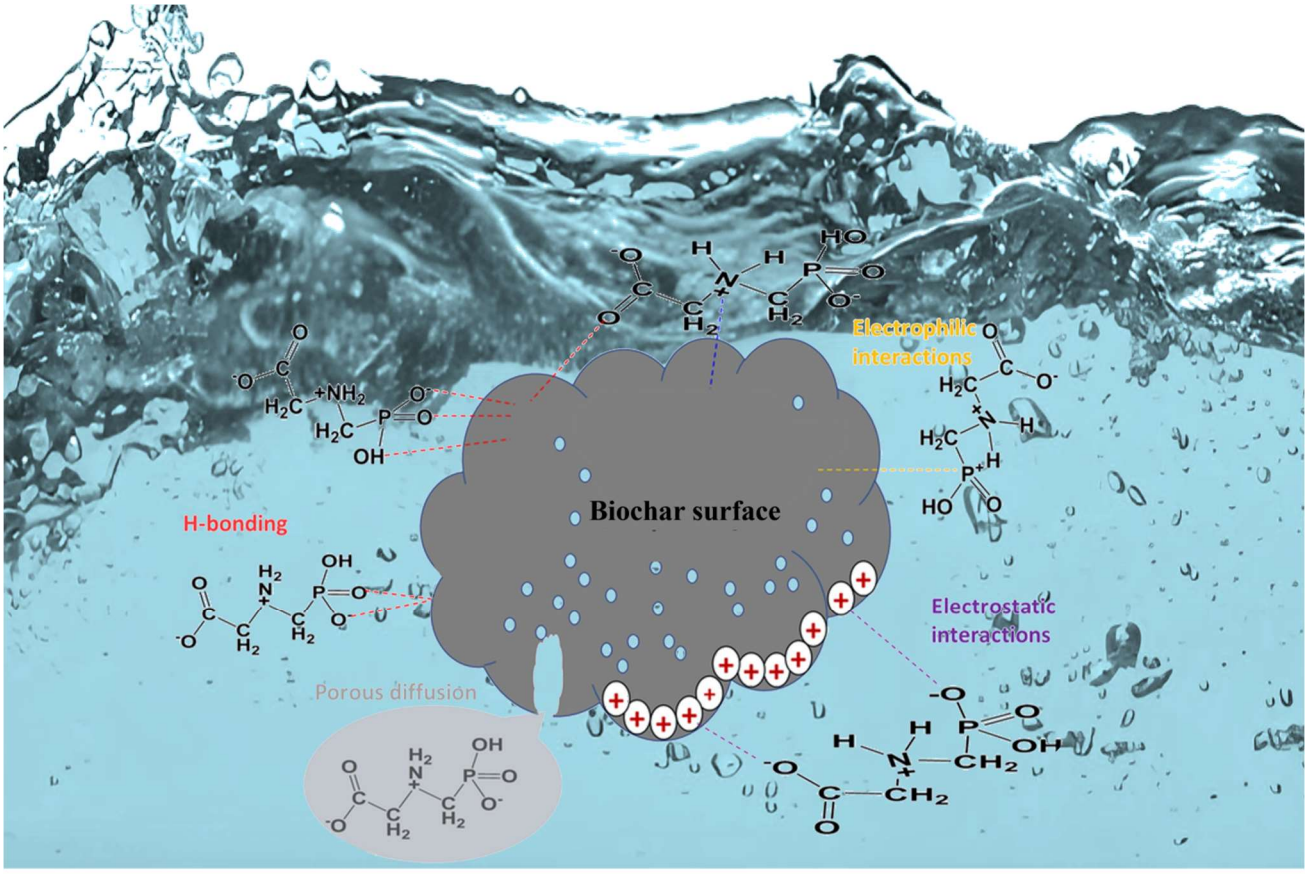

Figure 9. The mechanism of glyphosate removal from solution by adsorption method.

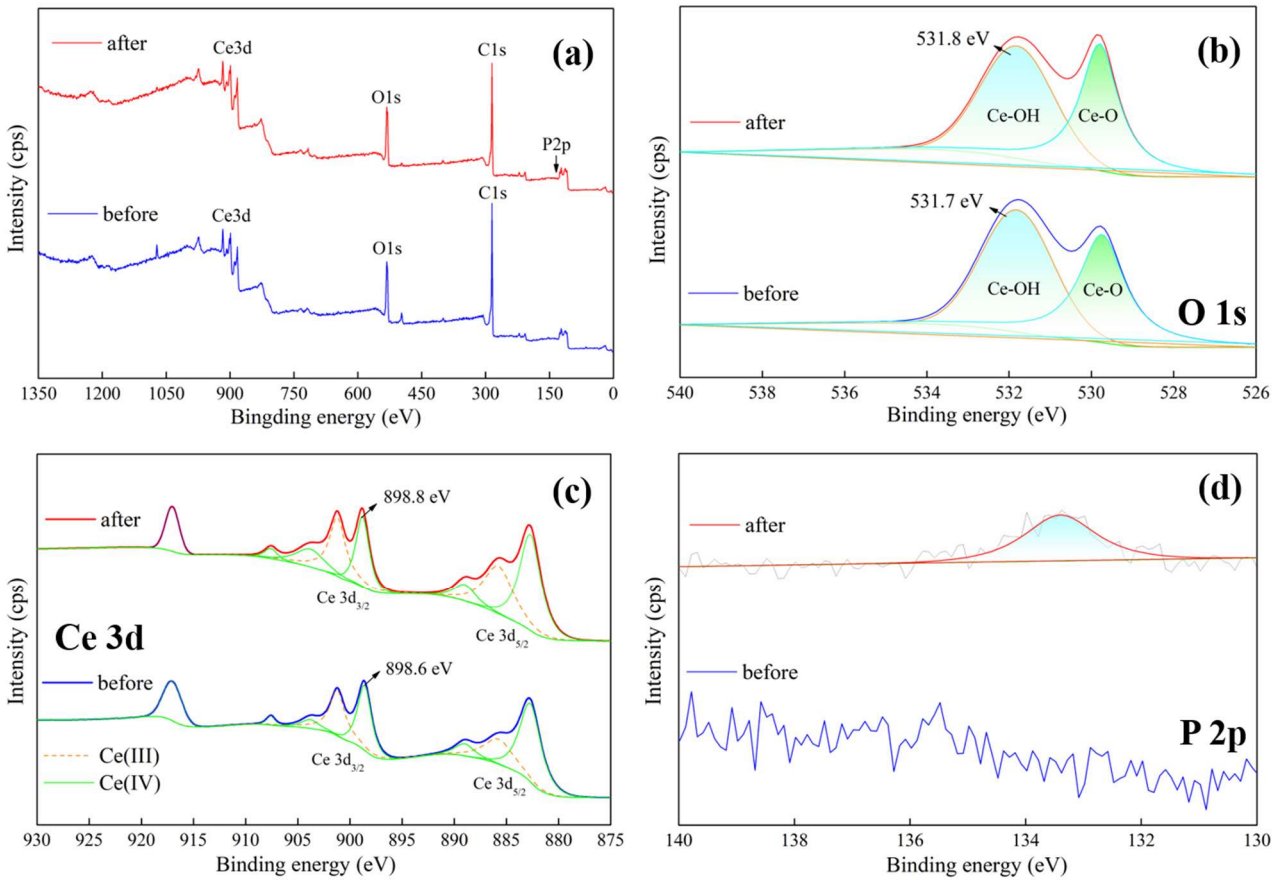

Figure 10. XPS survey spectra (**a**), O 1s (**b**), Ce 3d (**c**), P 2p (**d**) of CeO_2/WHBC-3 before and after adsorption.

4. Conclusions

The adsorbent CeO_2/WHBC, characterized by its high adsorption capacity and selectivity for glyphosate, was synthesized via an in-situ precipitation method at a pH of 12.0. The adsorption of glyphosate onto CeO_2/WHBC followed the Langmuir model and a second-order kinetic model, reaching completion within 30 min and achieving a maximum adsorption capacity of 126.3 $mg \cdot g^{-1}$. This material exhibited superior performance under acidic conditions and retained its adsorption capabilities after three regeneration cycles. The presence of most co-existing ions had a negligible effect on glyphosate adsorption on CeO_2/WHBC. XPS analyses indicated that electrostatic attraction and inner space complexation were the primary mechanisms driving glyphosate adsorption on CeO_2/WHBC. Given its outstanding adsorption properties, CeO_2-loaded biochar material holds great promise for the removal of glyphosate from industrial wastewater.

Acknowledgment

The authors express gratitude to the Joint Fund of National Natural Science Foundation (U24A2094), Hubei Natural Science Foundation Innovation and Development Joint Fund (2024AFD138), Hubei Three Gorges Laboratory Open Fund (SK240009) and Graduate Education Teaching Reform project of Wuhan Institute of Technology (NO. 2023JYXM09).for providing financial support for this study.

Author Contributions

B.Z.: Writing-original draft, Methodology, Investigation, Datacuration, Conceptualization. R.W.: Validation, Investigation. J.W.: Writing—review& editing, Formal analysis, Data curation. J.Y.: Writing—review & editing. Project administration, Funding acquisition. X.L.: MethodologyFormal analysis. L.G.: Resources. Y.C.: Resources. Q.Z.: Resources. C.X.: Resources. R.C.: SupervisionResources, Project administration.

Ethics Statement

Not applicable.

Informed Consent Statement

Not applicable.

Data Availability Statement

Data will be made available on request.

Funding

The work is funded by Joint Fund of National Natural Science Foundation (U24A2094), Hubei Natural Science Foundation Innovation and Development Joint Fund (2024AFD138), Hubei Three Gorges Laboratory Open Fund (SK240009) and Graduate Education Teaching Reform project of Wuhan Institute of Technology (NO. 2023JYXM09).

Declaration of Competing Interest

The authors declare that they have no known competing financial interests or personal relationships that could have appeared to influence the work reported in this paper.

References

1. Khoury GA, Gehris TC, Tribe L, Torres Sanchez RM, dos Santos Afonso M. Glyphosate adsorption on montmorillonite: An experimental and theoretical study of surface complexes. *Appl. Clay Sci.* **2010,** 50, 167–175. doi:10.1016/j.clay.2010.07.018.
2. Diel JC, Franco DSP, Igansi AV, Cadaval TRS, Jr., Pereira HA, Nunes IS, et al. Green synthesis of carbon nanotubes impregnated with metallic nanoparticles: Characterization and application in glyphosate adsorption. *Chemosphere* **2021**, *283*, 131193. doi:10.1016/j.chemosphere.2021.131193.
3. Liu R, Xie Y, Cui K, Xie J, Zhang Y, Huang Y. Adsorption behavior and adsorption mechanism of glyphosate in water by amino-MIL-101(Fe). *J. Phys. Chem. Solids* **2022**, *161,* 110403. doi:10.1016/j.jpcs.2021.110403.
4. Herath GAD, Poh LS, Ng WJ. Statistical optimization of glyphosate adsorption by biochar and activated carbon with response surface methodology. *Chemosphere* **2019**, *227*, 533–540.
5. Rallet D, Paltahe A, Tsamo C, Loura B. Synthesis of clay-biochar composite for glyphosate removal from aqueous solution. *Heliyon* **2022**, *8*, e09112. doi:10.1016/j.heliyon.2022.e09234.
6. Sen K, Mondal NK. Statistical optimization of glyphosate adsorption by silver nanoparticles loaded activated carbon: Kinetics, isotherms and thermodynamics. *Environ. Nanotechnol. Monit. Manag.* **2021,** 16, 100547. doi:10.1016/j.enmm.2021.100547.
7. Sittiwong J, Hiruntrakool K, Rasrichai A, Opasmongkolchai O, Srifa P, Nilwanna K, et al. Insights into glyphosate adsorption on Lewis acidic zeolites from theoretical modelling. *Micropor. Mesopor. Mater.* **2022**, *341*, 112083. doi:10.1016/j.micromeso.2022.112083.
8. Zavala-Robles K, Ramos-Ibarra J, Franco Rodriguez N, Zamudio-Ojeda A, Cavazos-Garduño A, Serrano-Niño J. Assessment of chitosan-based adsorbents for glyphosate removal. *J. Environ. Sci. Health B* **2024**, *59*, 62–71. doi:10.1080/03601234.2023.2291980.
9. Doan THY, Nguyen TTT, Kieu TT, Hoang DT, Vu TLC, Le TS, et al. Modification of bio-zeolite greenly synthesized from rice husk and application in adsorptive removal of herbicide glyphosate. *Mater. Chem. Phys.* **2024**, *316*, 129108. doi:10.1016/j.matchemphys.2024.129108.
10. Ma CM, Yang BY, Hong GB. Husk of Agarwood Fruit-Based Hydrogel Beads for Adsorption of Cationic and Anionic Dyes in Aqueous Solutions. *Molecules* **2021**, *26*, 1437. doi:10.3390/molecules26051437.
11. Diao ZH, Chu W. FeS_2 assisted degradation of atrazine by bentonite-supported nZVI coupling with hydrogen peroxide process in water: Performance and mechanism. *Sci. Total Environ.* **2021**, *754*, 142155. doi:10.1016/j.scitotenv.2020.142155.
12. Pan X, Gu Z, Chen W, Li Q. Preparation of biochar and biochar composites and their application in a Fenton-like process for wastewater decontamination: A review. *Sci. Total Environ.* **2021**, *754*, 142104. doi:10.1016/j.scitotenv.2020.142104.
13. Shi W, Wang H, Yan J, Shan L, Quan G, Pan X, et al. Wheat straw derived biochar with hierarchically porous structure for bisphenol A removal: Preparation, characterization, and adsorption properties. *Sep. Purif. Technol.* **2022**, *289*, 120796. doi:10.1016/j.seppur.2022.120796.

14. Zhang F, Wang X, Yin D, Peng B, Tan C, Liu Y, et al. Efficiency and mechanisms of Cd removal from aqueous solution by biochar derived from water hyacinth (*Eichornia crassipes*). *J. Environ. Manag.* **2015**, *153*, 68–73. doi:10.1016/j.jenvman.2015.01.043.
15. Yao XW, Chen X, Chen ML, Feng NJ, Tong LY, Yi YQ, et al. Removal of pesticide acetamiprid using KOH activated biochar derived from crayfish shell: Behavior and mechanism. *Process Saf. Environ.* **2024**, *186*, 808–818. doi:10.1016/j.psep.2024.04.076.
16. Wang J, Liao ZW, Ifthikar J, Shi LR, Chen ZQ, Chen ZL. One-step preparation and application of magnetic sludge-derived biochar on acid orange 7 removal via both adsorption and persulfate based oxidation. *RSC Adv.* **2017**, *7*, 18696–18706. doi:10.1039/C7RA01425B.
17. Wang J, Liao ZW, Ifthikar J, Shi LR, Du YN, Zhu JY, et al. Treatment of refractory contaminants by sludge-derived biochar/persulfate system via both adsorption and advanced oxidation process. *Chemosphere* **2017**, *185*, 754–763. doi:10.1016/j.chemosphere.2017.07.084.
18. Wang J, Shen M, Gong Q, Wang XH, Cai JY, Wang SL, et al. One-step preparation of ZVI-sludge derived biochar without external source of iron and its application on persulfate activation. *Sci. Total Environ.* **2020**, *714*, 136728. doi:10.1016/j.scitotenv.2020.136728.
19. Wang J, Cai JY, Zhou XQ, Wang SQ, Luo F, Yang L, et al. Accelerating of Fe^{2+} regeneration in Fenton reaction by biochar: Pivotal roles of carbon defects as electron donor and shuttle. *Sep. Purif. Technol.* **2025**, *354*, 128945. doi:10.1016/j.seppur.2024.128945.
20. Yan L, Dong FX, Lin X, Zhou XH, Kong LJ, Chu W, et al. Insights into the removal of Cr(VI) by a biochar-iron composite from aqueous solution: Reactivity, kinetics and mechanism. *Environ. Technol. Inno.* **2021**, *24*, 102057. doi:10.1016/j.eti.2021.102057.
21. Dong FX, Yan L, Zhou XH, Huang ST, Liang JY, Zhang WX, et al. Simultaneous adsorption of Cr(VI) and phenol by biochar-based iron oxide composites in water: Performance, kinetics and mechanism. *J. Hazard. Mater.* 2**021**, *416*, 125930. doi:10.1016/j.jhazmat.2021.125930.
22. Chen X, Yao XW, Diao Y, Liu H, Chen ML, Feng NJ, et al. Simultaneous removal of triadimefon and dinotefuran by a new biochar-based magnesium oxide composite in water: Performances and mechanism. *Sep. Purif. Technol.* **2024**, *336*, 126213. doi:10.1016/j.seppur.2023.126213.
23. Ban SE, Lee EJ, Lim DJ, Kim IS, Lee JW. Evaluation of sulfuric acid-pretreated biomass-derived biochar characteristics and its diazinon adsorption mechanism. *Bioresour. Technol.***2022**, *348*, 126828. doi:10.1016/j.biortech.2022.126828.
24. Chu G, Zhao J, Huang Y, Zhou D, Liu Y, Wu M, et al. Phosphoric acid pretreatment enhances the specific surface areas of biochars by generation of micropores. *Environ. Pollut.* **2018**, *240*, 1–9. doi:10.1016/j.envpol.2018.04.003.
25. Mood SH, Ayiania M, Jefferson-Milan Y, Garcia-Perez M. Nitrogen doped char from anaerobically digested fiber for phosphate removal in aqueous solutions. *Chemosphere* **2020**, *240*, 124889. doi:10.1016/j.chemosphere.2019.124889.
26. Jin H, Capareda S, Chang Z, Gao J, Xu Y, Zhang J. Biochar pyrolytically produced from municipal solid wastes for aqueous As(V) removal: Adsorption property and its improvement with KOH activation. *Bioresour. Technol.* **2014**, *169*, 622–629. doi:10.1016/j.biortech.2014.06.103.
27. Wang J, Shen M, Wang HL, Du YS, Zhou XQ, Liao ZW, et al. Red mud modified sludge biochar for the activation of peroxymonosulfate: Singlet oxygen dominated mechanism and toxicity prediction. *Sci. Total Environ.* **2020**, *740,* 140388. doi:10.1016/j.scitotenv.2020.140388.
28. Mood SH, Ayiania M, Cao H, Marin-Flores O, Milan YJ, Garcia-Perez M. Nitrogen and magnesium Co-doped biochar for phosphate adsorption. *Biomass Convers. Biorefin.* **2024**, *14*, 5923–5942. doi:10.1007/s13399-021-01404-1.
29. Jiang X, Ouyang Z, Zhang Z, Yang C, Li X, Dang Z, et al. Mechanism of glyphosate removal by biochar supported nano-zero-valent iron in aqueous solutions. *Colloids Surf. A Physicochem. Eng. Asp.* **2018**, *547*, 64–72. doi:10.1016/j.colsurfa.2018.03.041.
30. Huang Y, Li S, Chen J, Zhang X, Chen Y. Adsorption of Pb(II) on mesoporous activated carbons fabricated from water hyacinth using H_3PO_4 activation: Adsorption capacity, kinetic and isotherm studies. *Appl. Surf. Sci.* **2014**, *293,* 160–168. doi:10.1016/j.apsusc.2013.12.123.
31. Fu H, Ma S, Zhao P, Xu S, Zhan S. Activation of peroxymonosulfate by graphitized hierarchical porous biochar and MnFe2O4 magnetic nanoarchitecture for organic pollutants degradation: Structure dependence and mechanism. *Chem. Eng. J.* **2019**, *360,* 157–170. doi:10.1016/j.cej.2018.11.207.
32. Chen Q, Zheng J, Yang Q, Dang Z, Zhang L. Insights into the Glyphosate Adsorption Behavior and Mechanism by a $MnFe_2O_4$@Cellulose-Activated Carbon Magnetic Hybrid. *ACS Appl. Mater. Interfaces* **2019**, *11*, 15478–15488. doi:10.1021/acsami.8b22386.
33. Wang J, Cai JY, Wang SQ, Zhou XQ, Ding XT, Ali J, et al. Biochar-based activation of peroxide: Multivariate-controlled performance, modulatory surface reactive sites and tunable oxidative species. *Chem. Eng. J.* **2022**, *428*, 131233. doi:10.1016/j.cej.2021.131233.
34. Wu B, Lo IMC. Surface Functional Group Engineering of CeO2 Particles for Enhanced Phosphate Adsorption. *Environ.*

Sci. Technol. **2020**, *54*, 4601–4608. doi/10.1021/acs.est.9b06812.
35. Qian H, Yang J, Hu B, Zhang B, Wang Y, Liu J. Partially reduced CeO_2/C@CNT with high oxygen vacancy boosting phosphate adsorption as CDI anode. *Sep. Purif. Technol.* **2023**, *306*, 122557. doi:10.1016/j.seppur.2022.122557.
36. Ioannou ME, Pouroutzidou GK, Chatzimentor I, Tsamesidis I, Florini N, Tsiaoussis I, et al. Synthesis and Characterization of Cerium Oxide Nanoparticles: Effect of Cerium Precursor to Gelatin Ratio. *Appl. Sci.* **2023**, *13*, 2676. doi:10.3390/app13042676.
37. Deng S, Liu H, Zhou W, Huang J, Yu G. Mn-Ce oxide as a high-capacity adsorbent for fluoride removal from water. *J. Hazard. Mater.* **2011**, *186,* 1360–1366.
38. Mayakaduwa SS, Kumarathilaka P, Herath I, Ahmad M, Al-Wabel M, Ok YS, et al. Equilibrium and kinetic mechanisms of woody biochar on aqueous glyphosate removal. *Chemosphere* **2016**, *144*, 2516–2521. doi:10.1016/j.chemosphere.2015.07.080.
39. Herath I, Kumarathilaka P, Al-Wabel MI, Abduljabbar A, Ahmad M, Usman ARA, et al. Mechanistic modeling of glyphosate interaction with rice husk derived engineered biochar. *Micropor. Mesopor. Mater.* **2016**, *225*, 280–288. doi:10.1016/j.micromeso.2016.01.017.
40. Diel JC, Franco DSP, Nunes IS, Pereira HA, Moreira KS, Burgo TAL, et al. Carbon nanotubes impregnated with metallic nanoparticles and their application as an adsorbent for the glyphosate removal in an aqueous matrix. *J. Environ. Chem. Eng.***2021**, *9*, 105178. doi:10.1016/j.jece.2021.105178.
41. Naghdi S, Brown E, Zendehbad M, Duong A, Ipsmiller W, Biswas S, et al. Glyphosate Adsorption from Water Using Hierarchically Porous Metal-Organic Frameworks. *Adv. Funct. Mater.* **2023**, *33*, 2213862. doi:10.1002/adfm.202213862.
42. Wang H, Zhong Y, Yu H, Aprea P, Hao S. High-efficiency adsorption for acid dyes over CeO_2 xH_2O synthesized by a facile method. *J. Alloys Compd.* **2019**, *776*, 96–104. doi:10.1016/j.jallcom.2018.10.228.
43. Wang Y, Chen X, Yan J, Wang T, Xie X, Yang S. Efficient removal arsenate from water by biochar-loaded Ce^{3+}-enriched ultra-fine ceria nanoparticles through adsorption-precipitation. *Sci. Total Environ.* **2021**, *794*, 148691. doi:10.1016/j.scitotenv.2021.148691.
44. Wang Y, Xie X, Chen X, Huang C, Yang S. Biochar-loaded Ce^{3+}-enriched ultra-fine ceria nanoparticles for phosphate adsorption. *J. Hazard. Mater.* **2020**, *396*, 122626. doi:10.1016/j.jhazmat.2020.122626.
45. Yi Y, Luo J, Fang Z. Magnetic biochar derived from Eichhornia crassipes for highly efficient Fenton-like degradation of antibiotics: Mechanism and contributions. *J. Environ. Chem. Eng.* **2021**, *9*, 106258. doi:10.1016/j.jece.2021.106258.
46. Yue X, Zhang T, Yang D, Qiu F. Direct separation of phosphate under highly acidic conditions using MnO_2@CeO_2 nanowires membrane. *Chem. Eng. Process. Process Intensif.* **2022**, *177*, 108986. doi:10.1016/j.cep.2022.108986.
47. Kumaran C, Baskaran I, Sathyaseelan B, Senthilnathan K, Manikandan E, Sambasivam S. Effect of doping of iron on structural, optical and magnetic properties of CeO_2 nanoparticles. *Chem. Phys. Lett.* **2022**, *808*, 140110. doi:10.1016/j.cplett.2022.140110.
48. Ko YG, Do T, Chun Y, Kim CH, Choi US, Kim JY. CeO_2-covered nanofiber for highly efficient removal of phosphorus from aqueous solution. *J. Hazard. Mater.* **2016**, *307,* 91–98. doi:10.1016/j.jhazmat.2015.12.060.
49. Joshy D, Chakko S, Ismail YA, Periyat P. Surface basicity mediated rapid and selective adsorptive removal of Congo red over nanocrystalline mesoporous CeO_2. *Nanoscale Adv.* **2021**, *3,* 6704–6718. doi:10.1016/j.jhazmat.2015.12.060.
50. Zhou RY, Yu JX, Chi RA. Selective removal of phosphate from aqueous solution by MIL-101(Fe)/bagasse composite prepared through bagasse size control. *Environ. Res.* **2020**, *188*, 109817. doi:10.1016/j.envres.2020.109817.
51. Yamaguchi NU, Bergamasco R, Hamoudi S. Magnetic $MnFe_2O_4$-graphene hybrid composite for efficient removal of glyphosate from water. *Chem. Eng. J.* **2016**, *295*, 391–402. doi:10.1016/j.cej.2016.03.051.
52. Yu P, Li X, Zhang X, Zhou H, Xu Y, Sun Y, et al. Insights into the glyphosate removal efficiency by using magnetic powder activated carbon composite. *Sep. Purif. Technol.* **2021**, *254*, 117662. doi:10.1016/j.seppur.2020.117662.
53. Tran HN, You SJ, Hosseini-Bandegharaei H, Chao HP. Mistakes and inconsistencies regarding adsorption of contaminants from aqueous solutions: A critical review. *Water Res.* **2017**, *120,* 88–116. doi:10.1016/j.watres.2017.04.014.